Multimed Tools Appl (2017) 76:18955–18984
DOI 10.1007/s11042-017-4475-6

DeepKnuckle: revealing the human identity

Gaurav Jaswal[1] · Aditya Nigam[2] · Ravinder Nath[1]

Received: 21 September 2016 / Revised: 30 December 2016 / Accepted: 1 February 2017 /
Published online: 21 February 2017

Abstract Identification and authentication are ubiquitous questions which pan across various systems. In certain domains, they are of paramount importance. Like, security forces deploy various human identifications systems to discern potential wrongdoers. They constitute a vital part of various government social welfare schemes. The efficacy of the schemes is greatly impacted by them. Being pervasive and eminent, they demand more dedicated and focused research. Now-a-days, most of the systems incorporate a biometric system to address identification and authentication. The biometric system employs disparate traits like face, signature, iris, fingerprint, palmprint, speech, etc. for identification and authentication. A biometric trait must possess the following fundamental aspects; It should be able to identify an individual uniquely. For an individual, it should be consistent. To acquire it should be easy, cost-effective, time-efficient and automated. On such account, fingerprint trait is of outstanding merit. It has been widely studied and is an integral part of the many present biometric systems. However, fingerprints are subject to occupational hazard. The fingerprint is of abysmal quality for hand labourer, blacksmith, etc. due to the nature of their work. If a fingerprint based biometric system has a large number of such users then its precision is greatly affected. In such scenario, an alternate is to use finger-knuckle-print which possess almost comparable feature as fingerprint while being unaffected by such occupational hazards. In this paper, we propose a novel finger-knuckle-print based biometric system which could be deployed where a large number of user base is rural. Initially, ROI of finger knuckle image

✉ Gaurav Jaswal
gauravjaswal@nith.ac.in

Aditya Nigam
aditya@iitmandi.ac.in

Ravinder Nath
nath@nith.ac.in

[1] National Institute of Technology, Hamirpur, 177005, India

[2] Indian Institute of Technology, Mandi, 175005, India

has been extracted, enhanced and transformed using the proposed Bubble ordinal pattern (BOP), STAR ordinal pattern (SOP), and Image ray transform (IRT) based locally adapted procedures. A novel DeepMatching technique has been used to perform non-rigid distortion free matching between multiple features of two Finger Knuckle Images (FKI). Finally, the performance of proposed system has been evaluated using score level fusion rule, revealing improvement in the results.

Keywords Biometrics · Finger knuckle print · Bubble ordinal pattern · Star ordinal pattern · Image ray transform · DeepMatching

List of Abbreviations

CLAHE	Contrast Limited Adaptive Histogram Equalization
FKP	Finger Knuckle Print
FKI	Finger Knuckle Image
MCP	Meta Carpo Phalangeal
PIP	Proximal Inter Phalangeal
DIP	Distal Inter Phalangeal
CNN	Convolution Neural Network
GPU	Graphics Processing Unit
PolyU	The Hong Kong Polytechnic University
PCA	Principal Component Analysis
ICA	Independent Component Analysis
LDA	Linear Discriminant Analysis
CRR	Correct Recognition Rate
EER	Equal Error Rate
ROC	Receiver Operating Characteristics
FAR	False Acceptance Rate
FRR	False Rejection Rate
ROI	Region of Interest
SIFT	Scale Invariant Feature Transform
SURF	Speeded Up Robust Features
BLPOC	Band Limited Phase Only Correlation
LBP	Local Binary Pattern
LDP	Local Direction Pattern
HOG	Histogram of Oriented Gradients
DI	Discriminative Index
FTE	Failure to Enroll Rate
BOP	Bubble Ordinal Pattern
SOP	Star Ordinal Pattern
l_{BOP}	Longitudinal Bubble Ordinal Pattern
t_{BOP}	Transverse Bubble Ordinal Pattern
l_{SOP}	Longitudinal Star Ordinal Pattern
t_{SOP}	Transverse Star Ordinal Pattern
IRT	Image Ray Transform
TIR	Total Internal Reflection
KCP_{lBOP}	Knuckle Code Longitudinal Bubble Ordinal Pattern
KCP_{tBOP}	Knuckle Code Transverse Bubble Ordinal Pattern

KCP_{lSOP}	Knuckle Code Longitudinal Star Ordinal Pattern
KCP_{tSOP}	Knuckle Code Transverse Star Ordinal Pattern
LI	Left Index
LM	Left Middle
RI	Right Index
RM	Right Middle
NIST	National Institute of Standards and Technology
NIFQ	NIST Fingerprint Image Quality
IIT	Indian Institute of Technology
M_{kl}	Middle Knuckle Line
M_{kp}	Middle Knuckle Point
I_T	Knuckle Image
n_i	Refractive Index

1 Introduction

Traditional authentication and identification methods are based on features such as ID card, tokens, passwords and PIN codes. These features can be easily duplicated, cracked or stolen. An alternative to such systems is a biometric system that facilitates the process to recognize an individual by his/her unique physiological and behavioral characteristics. The advantages of a biometric system are: no prerequisite to remember whatever, not easy to manipulate or steal, difficult to forge or share, and testify the occurrence of genuine user at the time of enrollment. However, not every physiological or behavioral characteristic meet the requirements of being a biometric trait. A characteristic has to satisfy certain properties such as uniqueness, universality, collectivity, circumvention and permanence [14, 15]. Some features such as color of eye/skin/hair, age, scars, gender and height are known as soft biometrics. It has been observed that individuals cannot be distinguished on the basis of soft biometrics because these features may not be unique and stable. However, they improve the precision of the system when used in conjunction with physiological or behavioral biometrics traits. Illustrations of a few biometric traits such as face, signature, fingerprint, iris, speech, and palmprint are shown in Fig. 1. They have been presented in numerous civilian or forensic applications such as border crossing, e-banking, health care, and law enforcement [15]. The choice of a biometric characteristic depends on the exact requirements of

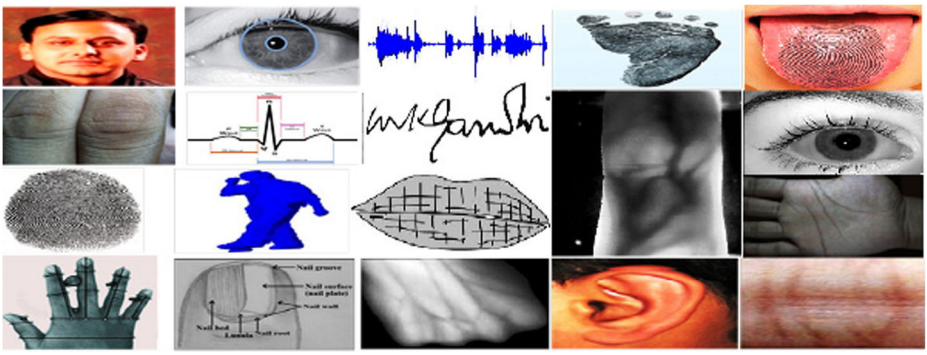

Fig. 1 Biometric Traits

the anticipated application [14]. It has been claimed that no biometric feature is superior to others or can replace any other but each one has its own pros and cons [4, 14] as mentioned in Table 1.

A biometric system can constitute of the following subsystems:

- Enrollment: Extracted features are saved in a database to register an individual.
- Verification: One-to-One matching that depends on a threshold (authentication).
- Identification: One-to-Many matching that reports top matching scores and corresponding top probable subjects (recognition).

Hand based biometric traits have been intensively studied to develop a consistent authentication system with higher precision, usability, and acceptance [4, 17]. Several hand biometric traits such as palm print [9], Inner Knuckle Print (IKP)[18], and Finger Knuckle Print (FKP) [5] have unique anatomical structures that can be captured with low cost and small size imaging devices (such as a webcam) without mounting extra hardware [5, 17]. These traits are present in various access control applications and captures around 60 % of market share of biometric systems [17].

1.1 Motivation

In several Asian countries, like India, more than 70 % of the population resides in rural areas. The laborers, and cultivators do substantial work and use their hands very roughly. This causes plenty of damage to their fingerprints permanently [32]. It has been observed that their quality of fingerprint is not very good. In such a scenario, the quality of FKP is unaffected because they are not used for any other purpose. Hence, it is less prone to injuries [6].

Table 1 Trait-wise Challenges and Issues

Trait	Motivation	Challenges	Issues
Fingerprint [5]	Easy collection, unique, economic sensor, less cooperative	Rotation and translation	Acceptance
Iris [28]	Highly discriminative and unique, expensive sensor, well protected	Segmentation, Motion blur, illumination, rotation	Cooperation, acquisition, acceptance
Palm print [12]	Contactless sensor, bigger ROI, unique	Rotation and translation	Cooperation, acquisition, acceptance
Hand Geometry [35]	Easy collection, cheap sensor, less cooperative	Rotation and translation	Acceptance
Face [9]	Non-intrusive, most obvious, universal, economic sensor	Pose, rotation expression, illumination, ageing	Acquisition
Finger Knuckle-Print [21]	Unique, cheap sensor discriminative, well protected,	Rotation and translation	Cooperation, acquisition, acceptance
Ear [25]	Non-intrusive, cheap sensor, universal, robust shape	Scale, rotation translation, illumination	Cooperation, acquisition, acceptance
Dorsal Hand Vein [22]	Non-intrusive, Expensive sensor, universal, robust shape	illumination	Cooperation, acquisition, acceptance

1.1.1 Knuckle print

The convex shape skin patterns which form around finger joints namely Meta Carpo Phalangeal (MCP), Proximal Inter Phalangeal (PIP), and Distal Inter Phalangeal (DIP), consist of highly rich lines and creases called as finger dorsal knuckle print (FKP) [18, 19]. The skin patterns are believed to be very unique, universal, and permanent [6]. They lie on the outer side of the finger and survive longer. Minutia and singular points of the fingerprint are known to fade over time in the hands of cultivators and laborers as shown in Fig. 2a. In such scenarios, FKP is a viable trait to be used for human identity recognition.

Quality comparison between FKP and fingerprint The prime goal of the proposed system is to come up with a solution applicable to rural areas. In this context, fingerprint and FKP based biometric systems are more suitable. A quality analysis of both of them reveals the superiority of FKP images in rural scenarios. In this work, efforts are being made to assess the image quality of FKP and fingerprint over a small in-house dataset of 10 individuals. Among them, 4 subjects were 55-64 years old and others were 40-45 years old. All of them belonged to rural Indian villages and were involved in very hard labor. To estimate the FKP quality, our previous work [32] has been used, while for fingerprint quality estimation publicly available NIST based $nfiq$ tool [2] has been used objectively. Our observation over such images clearly suggests that the fingerprint quality in this scenario lags behind FKP.

Likewise, palm provides a bigger ROI region, with more detailed features. However, there is a risk of size complexity [9]. Also, the geometrical features of hand/finger may not be unique for identification because they can change over time due to illness and other environmental factors [11]. On the other hand, dorsal hand veins have strong anti-forgery characteristics as the skin patterns underneath are actually unique and remain relatively stable through the adult age [22]. The FKP can be collected easily using ordinary, contactless cameras with lesser user co-operation [39]. The user failure to enroll (FTE) rate is lower as it is not associated with any fraud and criminal studies [32, 33]. Moreover, the dorsal knuckle patterns cannot be easily duplicated, and the possibility of information loss from this region is also less. But, there exist a big challenge to track the middle knuckle line for FKP registration because there might be deviations in spatial location of fingers during acquisition. Hence, it is concluded that a specific pre-processing, feature extraction and matching schemes are required to fully trace the curved shape features for higher FKP performance.

(a) Fingerprint Vs FKP (b) Nonlinear Distortion

Fig. 2 FKP motivation and challenges: (**a**) Quality based comparison of fingerprint (*top*) and knuckleprint (*bottom*) images of a person (**b**) Knuckleprint images of the same finger with different nonlinear distortions due to knuckle bending

1.1.2 Deep-matching: Multi-scale image matching technique

The multi-scale architecture of Deep-matching technique is inspired by functioning of Convolution Neural Network (CNN). The CNN models are made up of neurons with learn-able weights/biases and have shown tremendous improvements in image classification [10]. However, the Deep-matching technique does not create NN models to learn but this is a beautiful hierarchically inspired image matching paradigm. Basically, a local descriptor focuses only at the salient feature locations but match the deformable objects poorly. It has been observed that the Scale Invariant Feature Transform (SIFT) like features are unable to compute their pointwise dense correspondence. On the contrary, Deep-matching technique utilizes a quad tree based multilayer network that filters an image cell at different scales and improves the feature matching of non-rigid deformable as well as large displacement surfaces very accurately [41].

1.1.3 Contribution

The non-rigid and weakly textured regions of a FKI provides intricacies to FKP recognition. They are the major contributor towards false rejection in FKP based matches. Moreover, we argue that the central line tracking for FKP registration may not have uniformity and leads to the requirement of flexible ROI extraction. The deviations in spatial location of the same finger at the time of acquisition can be clearly seen as depicted in Fig. 2b. This type of intuition degrades the pointwise correspondence of deformable FKP patches. To handle such non-rigid deformation and large displacement in FKP image, we need to estimate correlation at several patch scales. The quad tree patch subdivision based Deep-matching algorithm can be seen as an ultimate solution. The contribution of this work can be summarized as follows: The ROI of raw FKP image is cropped by considering central knuckle point as reference and further its contrast is enhanced using Contrast Limited Adaptive Histogram Equalization (CLAHE). In the image enhancement, the additive noise is now assumed as multiplicative and has shown significant improvement. The novel image transformation schemes based on the ordinal relationship of two adjacent pixel gradient values, named as Bubble Ordinal Pattern (BOP) and Star Ordinal Pattern (SOP) are proposed to obtain the robust edge information. The resultant image is further processed using ray optics based Image Ray Transform (used first time to best of our knowledge) to strongly highlight the curved shape tubular features present in FKP image. Eventually, a high performance Deep-matching algorithm (which is a Graphics Processing Unit (GPU) based parallelized algorithm) has been used to address dense and non-rigid deformations in FKP images. The proposed system has been tested over a publicly available benchmark – The Hong Kong Polytechnic University (PolyU) FKP database [1] that consists of 7920 FKP images. Its performance has been measured in terms of computation time, discriminating index, Equal Error Rate (EER) and Correct Recognition Rate (CRR). The block diagram representation of the proposed FKP biometric system is shown in Fig. 3. To the best of our knowledge, there are very few related works existing in the literature which address the problem of large displacement and non linear distortion in FKP images as shown in Fig. 2b.

The rest of the article is organized into the following six main sections. Section 2 describes the FKP state-of-art work. In Section 3, ROI extraction, image enhancement, and image transformation schemes have been discussed. Section 4 highlights the role of feature extraction. The proposed matching strategy is discussed in Section 5. Then, experiment results are described in Section 6. Finally, the conclusions are summarized in the last section of this paper.

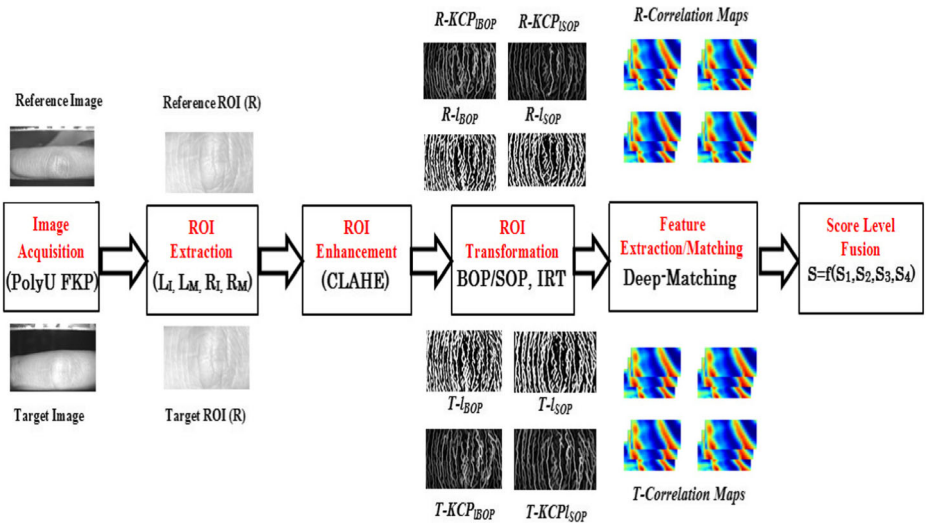

Fig. 3 The proposed framework for FKP based biometric system

2 Related work

The skin patterns such as creases, lines, and texture over finger knuckle surface have a lot of discrimination ability to be broadly recognized as a biometric identifier. Initially, due to lack of benchmark datasets and poor recognition rates, this area did not receive much attention and thus a limited number of works were reported till 2007. After that, immense efforts have been made in the area of FKP based personal authentication system. Majority-wise, region of interest (ROI) detection, feature extraction, and classification play an important role in FKP based personal recognition system. There are some additional requirements too, such as the size of the template, power intake, memory storage etc., but these cannot be achieved together. In this section, a state of art related to ROI extraction as well as feature extraction/classification techniques are presented.

2.1 ROI extraction

To segment and extract fixed size ROI from an original FKP image is a crucial stage and it really affects the final recognition accuracy. The existing methods extract ROI based upon local convexity characteristics of the skin patterns near major finger joint (PIP). Most of the existing techniques are tested against two publicly available datasets i.e., PolyU FKP dataset and IIT Delhi Finger Knuckle Image dataset.

In [29], a local coordinate system is established to align the images (PolyU FKP) and ROI is cropped for feature extraction. In this method, the curved lines on the two sides of the PIP joint are observed and then pixels over lines are encoded as a two tuple (1,-1) as per their convex directions. The convexity magnitude is measured to find the strength of principal curve. It is minimum around the center of PIP joint while maximum on left and right sides lines because FKP image is positioned horizontally. On that basis, the center position is considered to fix the Y- axis of the coordinate system and ROI of size (160×80) is cropped empirically. In [20], authors designed a novel ROI extraction algorithm by using contrast

enhanced and corrected skewed images. Subsequently, a center point based ROI detection and localization method for FKP images is given in [38]. This method is robust against finger displacement and rotation in the horizontal direction. In [32], the middle knuckle line and middle knuckle point are determined to extract the ROI of FKP image. The authors proposed a modified Gabor filter by adding curvature parameter to check the response of curved convex line features present around the major finger joint. It has been observed that the pixels over middle knuckle line have a maximum filter response because FKP structure is vertically symmetric. Finally, ROI is extracted on the basis of central knuckle point and found 95 % of accuracy over PolyU FKP dataset.

2.2 Feature extraction and classification

The conventional knuckle print recognition approaches can be categorized into the following groups: subspace methods, coding methods, texture analysis methods, and other image processing methods. In [7] an apparatus was developed to identify or verify individuals using their knuckle contours. In [18], the authors considered creases of finger inner surface for biometric identification. The matching was carried out using the normalized correlation function. In [36] the folds and creases on the finger outer surface were examined. The authors had employed Minolta 900/910 sensor to collect 3D finger samples, but it was quite an expensive, bulky, and slow processing device which limited its use in commercial or real time systems. In the following year, knuckle code based coding scheme for texture feature extraction was conceptualized [29]. During the same time, the authors [33] clubbed both the knuckle texture and geometrical features of hand, which were acquired by a peg-free and non-contact imaging setup. In [40], 2-D Gabor filter was employed to extract local orientation information, and saved it in a feature vector named competitive code. Likewise, the authors [24], modified the knuckle codes approach by applying radon transform on enhanced knuckle images and resulted in 1.14 % EER and 98.6 % rank one recognition rate. Additionally, [23] suggested a multi algorithmic approach based on matching scores of principal component analysis (PCA), linear discriminant analysis (LDA) and independent component analysis (ICA) with EER of 1.39 %. In [41], another significant method called as monogenic code (3 bit vector) which reflected the phase and orientation information in knuckle images was framed. Likewise, [42] improved their previous work by combining the magnitude (magnitude code) and the orientation information (improved competitive code). In another work [43], the authors have used a weighted sum rule to fuse local and global information to achieve optimum results. In [30], SIFT key points from Gabor filter based enhanced FKP images were extracted. In [6], knuckle texture had been used as an identifier in smartphone applications. In [31], efforts were made to compute FKP image quality attributes. In [11], score level fusion was adopted to integrate the obtained matching scores caused by fragility masks. In [37], the authors implemented a well-known local feature descriptor called as LBP over ROIs based FKP images. In [26], the authors performed matching over recovered minutiae samples by using minutiae cylindrical code, minutiae triangulation, and spectral minutiae based approaches. This section presented the various author's research work and highlights the following issues: The FKP is still a less examined biometric trait for a wide range of applications. There are few related works that exist in literature which tackle the problem of large displacement and non-rigid deformation in FKP images, as this leads to false rejections in the matching process. There is a lack of FKP databases in which images incorporate the real world situations such as variation in bending of fingers.

3 Pre-processing approach

In this section, a sub region of finger knuckle image near Proximal Inter Phalangeal joint (PIP) is extracted using a ROI extraction algorithm [32]. The raw ROI images are then enhanced using the CLAHE scheme to stabilize the effects of poor contrast and non-uniform illumination. Although, finger dorsal surface is rich with texture patterns but the curve shape lines are not very clear. So, ROI samples are transformed into a better visual representation by gradient ordinal relationship based encoding schemes. Subsequently, its ray tracing features are extracted with the help of IRT which gives more discriminative information.

3.1 FKP ROI extraction

The basic idea behind ROI extraction is to apply a curvature Gabor filter with modification in X coordinate to estimate the middle knuckle line M_{kl}, and middle knuckle point M_{kp} as described in (1). The raw FKP image is thresholded to get binarized image from which knuckle boundary is measured as shown in Fig. 4b. The knuckle region is taken out using Sobel edge detector and a strongly attached component assuming the solid knuckle boundary (horizontal axis) as shown in Fig. 4c. The knuckle area is retrieved back from the pixels within the defined knuckle boundary as given in Fig. 4d. To estimate the Middle Knuckle Line M_{kl}, the knuckle region can be considered symmetric around the middle knuckle line of phalangeal joint. Since, the convex shape lines are observed to be protuberant on left and right side of knuckle area, while curves near middle knuckle line do not possess the exact convex shape. This makes the efforts easy to spot middle knuckle line and midpoint. To visualize such a convex shaped texture, a knuckle filter using additive curvature parameter is designed, as shown in Fig. 4e. The filter response can be seen as a modified version of classic Gabor filter, with X and Y modulated as:

$$X = x \times cos\theta + y \times sin\theta + c(-x \times sin\theta + y \times cos\theta)^2; Y = -x \times sin\theta + y \times cos\theta \quad (1)$$

Several curved Gabor filters can be obtained by changing the value of curvature parameter (c) and distance parameter (d) between two flipped curved filters. Now, the knuckle area image is convolved with the specific curvature Gabor filter ($F^{0.01,30}$) which provided a better idea to measure the strength of convex shaped lines over the knuckle region. The column wise filter response is found maximum at the middle column and that position is considered as a middle knuckle line (vertical axis) as shown in Fig. 4f. To estimate the Middle

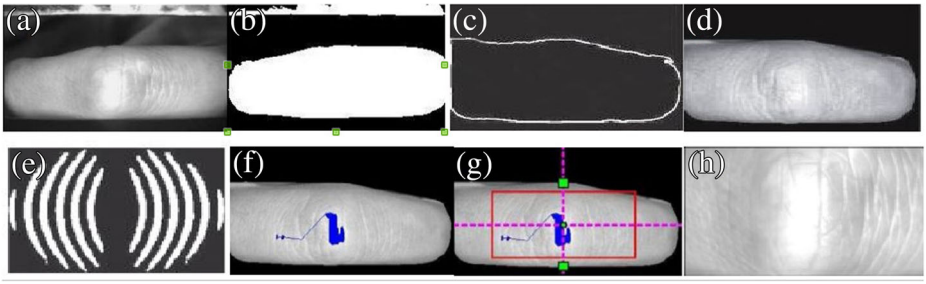

Fig. 4 FKP ROI extraction (**a**) Original, (**b**) Binary Sample, (**c**) Boundary, (**d**) FKP area, (**e**) Knuckle filter, (**f**) Filter response, (**g**) Localized ROI (**h**) Final ROI

Knuckle Point M_{kp}, the point at the center of the middle knuckle line with respect to the knuckle area is specified as the middle knuckle point. For locating a midpoint, top and bottom points of the middle knuckle line are assumed over knuckle area. Then, a ROI of fixed size is cropped from knuckle area image with consideration of M_{kl} and M_{kp} as shown in Fig. 4g. Finally, the knuckle ROI is normalized as given in Fig. 4h. Algorithm 1 summarizes the ROI extraction method.

Algorithm 1 Steps involved in FKP ROI Extraction

Require:
Raw FKP image I of size $m \times n$.
Ensure:
Cropped ROI image I_{ROI}, of size $(2 * l + 1) \times (2 * b + 1)$.
1: Perform image binarization I_E to I_B using clustering based Otsu thresholding;
2: Apply Sobel edge detection over I_B to get I_{sobel};
3: Detect the largest connected component in I_{sobel} as knuckle print boundary, $(FKP_{Bound}^{Original})$;
4: Abrade the extracted boundary $FKP_{Bound}^{Original}$ to obtain continuous FKP boundary, FKP_{Bound}^{Smooth};
5: Extract the knuckle area K_{area} = All pixels in image $I \in$ the $ConvexHull(FKP_{Bound}^{smooth})$;
6: Apply the modified Gabor filter $F_{kp}^{0.01,30}$ over all pixels $\in K_{area}$;
7: Binarize the filter response using $f * max$ as the threshold;
8: The middle knuckle line (M_{kl}), is considered which has maximum filter response;
9: The point at center over $M_{kl} \in K_{area}$, is defined as the middle knuckle point (M_{kp}).
10: The ROI (I_{ROI}) is cropped as size $(2 * l + 1) \times (2 * b + 1)$ from enhanced FKP image I_E, assumed M_{kp} as a middle point.

3.2 FKP ROI enhancement

The textured region of the knuckle print can be used for identification as it is unique for every individual. The finger dorsal signifies a fairly deformable surface, which results in uncertain reflections and illuminations. A ROI sample is partitioned into non overlapping fixed size cells (10×10). The cell size is selected empirically which ensures that mean of every cell almost indicates the coarse illumination of it. This mean of coarse illumination is expanded to the original ROI sample. The estimated illumination of every cell is divided from the corresponding cell of the original ROI and get a uniformly brightened ROI sample, as shown in Fig. 5b. Instead of using the full illumination value for this purpose, we have scaled down the value using f_{scale} (between 0 and 1). Now, the resulting ROI image is enriched using CLAHE, which improves the contrast in the texture without adding noise and increases the discriminative strength as shown in Fig. 5d. Further, the blocking effect is reduced using bi-linear interpolation. Finally, Weiner filtering is applied to smooth the boundaries between the blocks, and to minimize the additive noise as depicted in Fig. 5e.

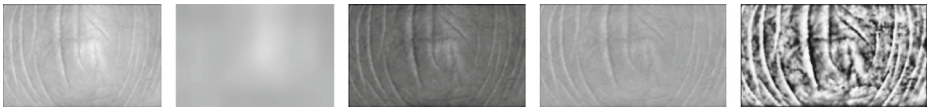

(a) I_{ROI} (b) Steady Ill. (c) En. (Additive) (d) En. (Multi.) (e) De-noised

Fig. 5 Proposed Image Enhancement for FKP images (Difference between Additive Vs Multiplicative noise can be observed from Fig. 5c and d)

Justification Here, our assumption is that noise is multiplicative in nature that increases brightness. The increase in overall performance adds merit to our assumption.

3.3 FKP ROI transformation

A key issue to efficiently measure the texture properties is to get the best texture representation. Recently, many robust methods such as LBP [3] have been developed for texture representation which threshold the neighborhood pixel with respect to a central pixel. In this work, the enhanced ROI sample is transformed using novel image transformation schemes namely Bubble Ordinal Pattern (BOP) and Star Ordinal Pattern (SOP). We propose BOP/SOP over first order image gradient which shows high level discriminative features. They provide robust transverse and longitudinal representations against variable illumination. This is due to the fact that gradient values are strong indication of the local edge information. Further, a ray tracing based mechanism has been used to enhance the detection of knuckle structural features relying strongly on their intensity. Image Ray Transform (IRT) basically highlights the knuckle convex hull strongly due to presence of high intensity epidermal texture around major finger joint. Algorithm 2 concludes the image transformation steps.

Algorithm 2 Image Transformation

Require:
Enhanced FKP image I_E of size $m \times n$.
Ensure:
Transformed images $(I_T)^{lBOP}$, and $(I_T)^{lSOP}$ of $m \times n$ size
1: Compute longitudinal (I_l) image gradients using Sobel edge detection kernel.
2: Apply BOP or SOP algorithm to compute the corresponding images l_{BOP} or l_{SOP} as follows:
- l_{BOP}= BOP (I_l)
- l_{SOP}= SOP (I_l)

3: Apply IRT over l_{BOP} and l_{SOP} so as to get the robust and noiseless KCP as follows:
- KCP_{lBOP} = IRT (l_{BOP})
- KCP_{lSOP} = IRT (l_{SOP})

4: Return
- $(I_T)^{lBOP} = KCP_{lBOP}$
- $(I_T)^{lSOP} = KCP_{lSOP}$

Comparison of proposed transformation with various existing transformation LBP [3] and CS-LBP [13] are originally defined over gray scale images (as shown in Fig. 6c, d), but we have observed that gray values as well as their locally computed ordinal relationship are very fragile, especially in the region where the texture is very elusive. On the other hand, they are not robust to illumination variation. Hence, in order to cater such issues, we have used the first order derivatives computed by difference operator. We propose the Bubble Ordinal Pattern (BOP) over first order gradient which can extract the high level discriminative features. To best of our knowledge, such Bubble pattern code (BOP) has never been considered previously. As compared to LBP, the BOP does not threshold with respect to center pixel. While, SOP is related to CS-LBP, but instead of 4-bit codes we have redundant them into 8 bit as they were not properly scaled into image representation. Thus, the key point to note here is that SOP/BOP computations are over the image gradients.

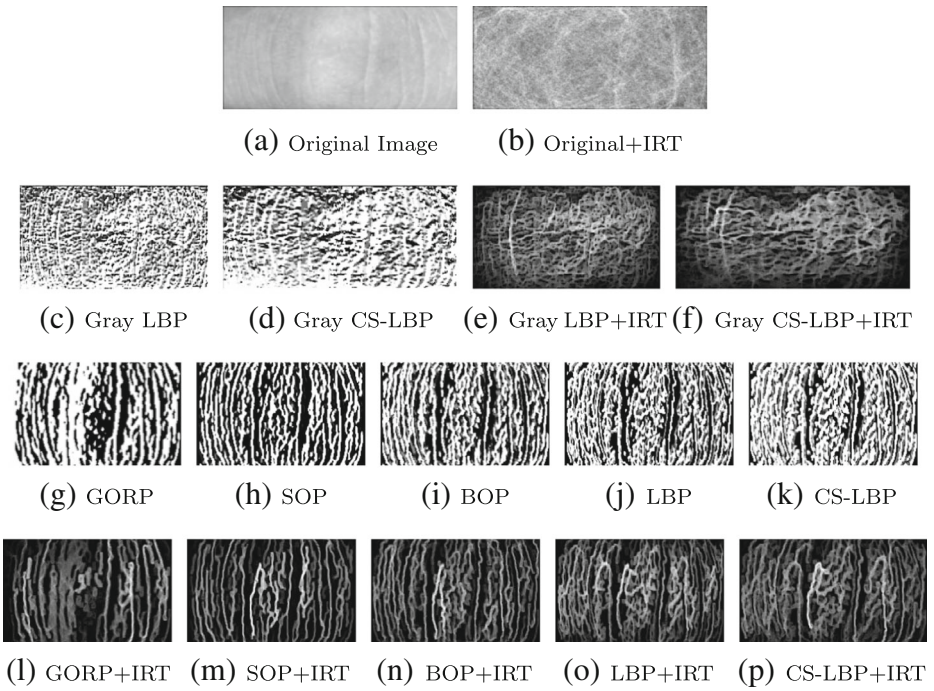

Fig. 6 Visual features based appearance analysis. Images are persented before and after applying various existing transformations. First row: Original and IRT applied images, Second row: Transformations over gray images, Third and Fourth row : Transformations over gradient images. Last row shows rich and enhanced FKP tabular structure extracted using IRT

Our motivation to work over gradient was that gradients are robust to variable illumination. Any gradient based ordinal relationship can be considered more robust as compared to any equivalent gray scale version. Since gradient values are involved, we have observed that automatically edges and their relationship gets most of the emphasis and finally got encoded into the proposed pattern (as shown in Fig. 6g-p). This encoding scheme not only becomes robust for variable illumination, but also very discriminative. Moreover in our current experimentation, we have monitored the behavior as well as visual image appearance as shown in Fig. 6, along with the performance of the proposed BOP/SOP codes presented in Section 6.6.

3.3.1 Bubble ordinal pattern (BOP)

The enhanced ROI samples are down-sampled to a fixed size in order to reduce computation time. The ROI samples are further processed by the proposed encoding schemes – Bubble Ordinal Pattern (BOP) and Star Ordinal Pattern (SOP). The computational steps related to BOP are mentioned in Algorithm 3 and transformed images are shown in Fig. 6h, i, m and n.

Transformation basis The opted Sobel kernel (9×9) can estimate thick and discriminative edges. It is a discrete differentiation operator which is a result of quantification of

the longitudinal and the transverse derivative approximations of the gradient of the image intensity function. The BOP computes the ordinal relationship of two adjacent pixel gradient values, specifically when neighbors have similar values. The gradient of any pixel will be +ve or −ve that is encoded into a bit either 1 or 0 coding value. Hence, such ordinal relationship encodes the type of edge that is passing trough the corresponding pixels. The proposed encoding mechanism utilizes Sobel longitudinal kernel to assign an 8-bit code (l_{BOP}) to every pixel based on the derivatives of eight neighbors. It has been observed that the obtained transverse derivatives are not very robust primarily due to the prominent longitudinal features present in the FKP images. Hence, after rigorous experiments, we have dropped transverse gradient (t_{BOP}) and other derived features from it.

Algorithm 3 BOP Algorithm

Require:
The image gradient (I_g) of size $w \times h$.
Ensure:
Encoded images I_{BOP} of size $(w-2) \times (h-2)$.

```
for u=1 to w-1 do
  for v=1 to h-1 do
    for k=1 to 8 do
      if G_k > G_{(k+1)%8} then
        BOP(u,v)[k] = 1
      else
        BOP(u,v)[k] = 0
      end if
    end for
  end for
end for
```

Transformation The bubble ordinal pattern based encoding evaluates BOP_{Code} for every pixel based on transverse and longitudinal derivatives of its eight neighbors as shown in Fig. 7a. Suppose that $E_{u,v}$ defines spatial location of $(u, v)^{th}$ pixel in an enhanced FKP ROI

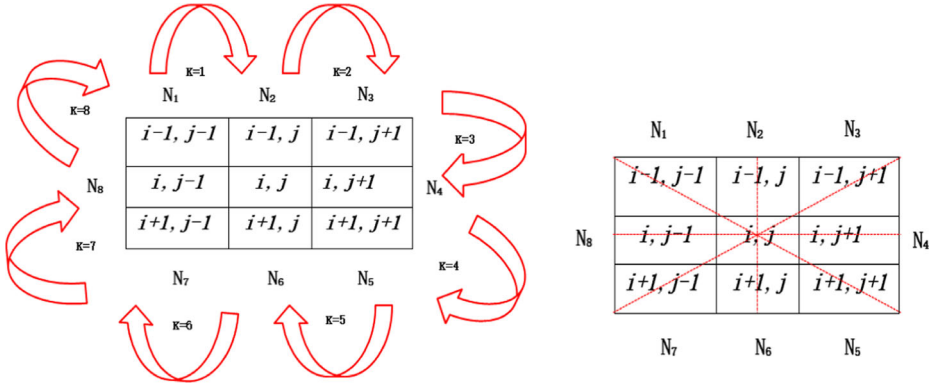

(a) BOP Pattern (b) SOP Pattern

Fig. 7 Neighborhood pattern considered for image transformation

sample. The obtained BOP_{Code} response for each pixel is an 8-bit binary number whose k^{th} bit is stipulated in (2):

$$BOP_{Code}(u,v)[k] = \begin{cases} 1, & \text{if } G_k > G_{k+1} \\ 0, & \text{otherwise} \end{cases} \quad (2)$$

where, G_K , k=1,2,3....8 represent the gradients of eight adjacent pixels positioned around $E_{u,v}$ with the use of transverse or longitudinal Sobel kernels. Therefore, l_{BOP} or t_{BOP} are basically BOP_{Code} based representation of entire pixels in a ROI sample as computed in step 2 of Algorithm 2.

Justification The basic assumption is that the pattern of edges within eight neighborhood of any pixel does not change abruptly because gradient values are robust in nature. Our motivation was not only to achieve illumination invariance (so using gradient) but also to get discrimination that has been achieved because the edges get more and more emphasis. The related BOP codes are shown in Fig. 8b, c.

3.3.2 STAR ordinal pattern (SOP)

Another encoding scheme, known as star ordinal pattern (SGORP), has been used [32]. In this scheme, gradient of a pixel is given either positive, negative or zero code based on its edge position. An 8 bit encoding scheme for every pixel is performed which considers diagonally opposite neighbors (as shown in Fig. 7b) together with upper and lower ones. The SOP_{Code} can be computed using the Algorithm 4. The related SOP codes are shown in Fig. 8d, e.

Algorithm 4 SOP Algorithm

Require:
The image gradient (I_g) of size $w \times h$.
Ensure:
Encoded images I_{SOP} of size $(w-2) \times (h-2)$.

```
for u=1 to w-1 do
  for v=1 to h-1 do
    i=1;k=1
    while k < 8 do
      if G_i > G_{(i+4)%8} then
        SOP(u,v)[k] = SOP(u,v)[k+1] = 1
      else
        SOP(u,v)[k] = SOP(u,v)[k+1] = 0
      end if
      i=i+1;k=k+2
    end while
  end for
end for
```

3.3.3 Image ray transform (IRT)

The transformed ROI knuckle image (I_T) consists of prominent curved lines, and stable structures than original ROI sample. The detection of specific structural features within an image is a challenging task in biometrics. The image ray transform (IRT) has been received significant consideration for structural feature detection empirically in medical imaging, and retinal vessel extraction. Based on the principal of ray optics, IRT technique uses the concept of tracing light rays through an image as depicted in Fig. 9. Hence, it mainly highlights the

(a) I_R (b) l_{BOP} (c) t_{BOP} (d) l_{SOP} (e) t_{SOP}

Fig. 8 BOP and SOP based Image Transformation and Encoding Schemes (Transversed components are discarded)

curvilinear structures such as tubes or curves as clearly evident from Fig. 6l-p. In this work, IRT is introduced for the first time, to best of our knowledge, to emphasize the curved (lines and creases) features from transformed FKP images as explicitly shown in Figs. 6 and 10. The transform treats an image pixel as a set of 2-D glass blocks with refractive indexes linked to intensity of the pixel and then casts a large number of rays through the image. The sequence of these rays is accumulated into an output image which emphasizes certain structural features. The route that a ray follows is often changed when propagating from one to another medium with different refractive indexes. Refraction of light at the surface of separation of two media can be better understood by the Snell's Law.

Justification FKP images have a significant amount of longitudinal textured patterns. These are thick curved features obtained after BOP or SOP transformations. One can observe from Fig. 10, that such features can be easily highlighted using proposed IRT transformation.

IRT implementation The IRT creates a magnified image as the way light reflects off curved features [8]. Take a transformed knuckle image (I_T) of size ($m \times n$). Then, a refractive index (n_i) value for the i^{th} pixel is computed as a function of its intensity (g).

$$n_i = 1 + \left(\frac{g}{255}\right)(n_{max} - 1) \tag{3}$$

whereas, n_{max} represents the maximum refractive index for a linear model. Next, the computation of the refractive index for randomly selected pixels is described. The algorithm traces a path through the pixels by emulating refraction and total internal reflection. Figure 9 visually explains the working of IRT. At each pixel the direction of normal is vertical. The blocks of distinct shades represent media with different refractive index.

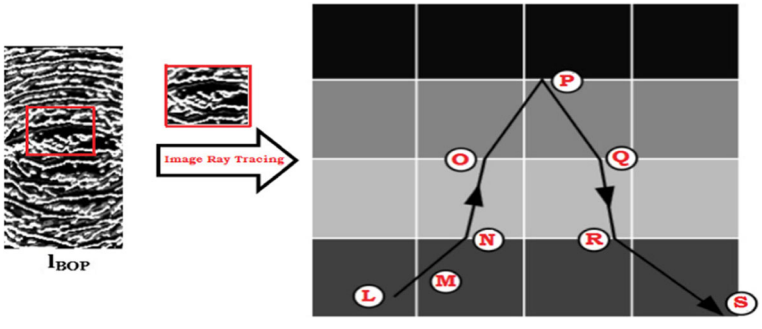

Fig. 9 A patch in the transformed image has been enlarged to explain Image Ray Tracing (IRT). Reflection, refraction and TIR happens in accordance to Snell's law

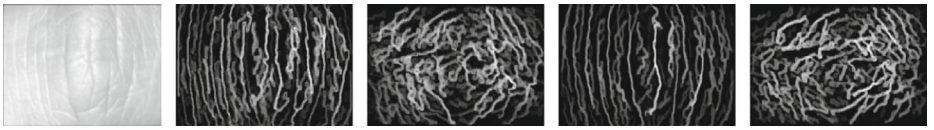

(a) I_R (b) KCP_{lBOP} (c) KCP_{tBOP} (d) KCP_{lSOP} (e) KCP_{tSOP}

Fig. 10 Image Ray Transformation (Transverse components are discarded)

- At point M, ray is initialized and travels towards B.
- At point N ($n_1 = n_2$), the ray continues to travel along the same direction.
- At point O ($n_1 < n_2$) or at point P ($n_1 > n_2$), refraction occurs and the light ray bends towards or away from the normal accordingly.
- At point Q ($\theta_i > \theta_c$), hence Total Internal Reflection (TIR) takes place and the ray reflects back into the same medium.
- At point R and S, the ray is an inverse replica of trace occurred at points O and P.
- At Q, eventually the ray exits. The tracing is allowed to continue until d reflections or refractions have undergone for each ray.

For each pixel, during the path tracing, if the refractive index of the next pixel is different, the θ_i (angle of incidence) and θ_r (angle of reflection) are calculated as:

$$\cos\theta_i = N.V \tag{4}$$

$$n = \frac{n_1}{n_2} \tag{5}$$

$$\cos\theta_r = \sqrt{1 - n^2(1 - N.V)} \tag{6}$$

where, N is the normal direction at each pixel, and V is a vector function of the initial direction vector at each pixel. The refraction vector, for the path to pass across boundary of pixel with different refractive index, is given as:

$$R_r = nV + (n(N.V) - \cos\theta_r)N \tag{7}$$

Likewise, if $\theta_i > \theta_c$ and $n_1 > n_2$, internal reflection will take place and hence the reflection vector is given by:

$$R_l = V - 2(N.V)N \tag{8}$$

The initial direction ϕ, to start the path tracing from each pixel, is randomly drawn from a uniform distribution. The overall methodology is outlined in Algorithm 5. Once the random rays from all the different points are cast, they start to trace in the whole image. The algorithm works in such a way that regions consisting of pixels with similar intensity values are emphasized. Thus, the tracing path of all those rays will finally converge and highlights the curved lines and creases from the rest of the image. Finally, when each ray has undergone a fixed number of refractions or reflections, the tracing of rays is ceased. The IRT implementation is mainly affected by maximum refractive index n_{max} (affects the number of segmented pixels), number of rays traced N (impacts the smoothness), and depth of ray tracing d (responsible for sharpness of the extracted features). Here, we set n_{max} value to 100, increased N value to 10000, and assume d value to 256. All parameters used in this work, have been listed and their default values with descriptions, as well as operating ranges are presented in Table 2.

Table 2 Description and nature of parameters

Parameter	Default value	Description	Operating Range	Nature
ROI Extraction				
Threshold	0.8	Otsu generated	0.3–0.9	High
c	0.01	The curvature term	0.0–0.04	Low
d	30	Distance between two gabor (Empirical)	0–50	Moderate
f	0.75	Fraction to binarize the response	0.45–0.95	High
CLAHE				
f_{scale}	0.5	Scaling down	0.4–0.6	Moderate
Block Size	10×10	Blocking, selected empirically	(8×8)–(16×16)	Low
BOP/SOP				
Sobel Kernel	9×9	Blocking to compute gradient (for thick features)	(3×3)–(11×11)	High
Image Ray Transform				
n_{max}	80	Maximum refractive index for linear model	20–120	Moderate
depth (d)	256	Tracing the ray to depth (d)	100–400	High
N	10000	Total number of points for experiment	1000–50000	High
DeepMatching				
Patch Size	4×4	Atomic Patch size	2×2–16×16	Low
Maxpooling	3×3	Max-pooling with a stride of 2	(3×3)–(9×9)	Low
Rectification	1.4	Gamma correction power factor	1–2	Moderate
Rotation	–26° to +26°	Rotational Invariance	–30° to +30°	High

Algorithm 5 Steps involved in IRT Algorithm

Require:
Encoded FKP image l_{BOP}, l_{SOP} of size $w \times h$.
Ensure:
Segmented image KCP_{lBOP}, KCP_{lSOP} of $w \times h$ size
1: Initialize N number of random points *(i,j)* and direction ϕ for each point from a uniform random distribution U
2: Defining the refractive index n_i for pixel at i^{th} position from equation 3
3: Let i^{th} location in image, direction and angle of incidence associated with it be denoted as X_i, ϕ_i and θ_i where $i \in \{1, 2, 3, ..., N\}$
4: Declaring variable *depth* to compare it with fixed parameter d in the transform.
5: Initialize depth=1
6: **for** i=1:N **do**
7: **while** $depth < d$ **do**
8: **if** $(\theta_i < \theta_c)||(n_i < n_{i+1})||(n_i > n_{i+1})$ **then**
9: Refraction occurs with vector $\mathbf{R}_r$
10: **else if** $\theta_i > \theta_c$ **then**
11: Reflection occurs with vector $\mathbf{R}_l$
12: **end if**
13: $depth = depth + 1$
14: **end while**
15: **end for**

4 Feature extraction

To perform image matching by using the set of local interest points is an important aspect of local texture descriptor based approaches. They perform compact vector representations of a local neighborhood, and are building blocks of many computer vision algorithms. Local features such as points, edges, blobs, and small image patches are distinctive and enable these methods to better handle scale change, rotation, and variable illumination [16]. The popular scale and rotation invariant local texture detectors are: Scale invariant feature transform (SIFT), Speeded up robust transform (SURF), Hessian Laplace, Harris detector, Local Energy based shape histogram, Local binary pattern (LBP), Local direction pattern (LDP), HOG, etc. The SIFT operator provides a robust solution to compare image patches with rich textures [27]. It performs a cascaded operation to match the robust key-points of the corresponding regions. But SIFT fails to match non-rigid deformable regions and image patches with weak or repetitive textures [34]. This is because the 4 cell grid in SIFT is completely rigid and it is not able to detect the non-linear deformations present in FKP images. In this section, the problem to match FKP images with non-rigid deformation and large displacement is highlighted.

5 DeepKnuckle : a novel knuckle identification framework

In contrast to descriptor matching approaches a dense, hierarchical algorithm to compute dense correspondence between images is introduced which is known as Deep Matching [34]. Deep Matching algorithm is based on a multi-stage architecture with 6 layers (depending on the image size), interleaving convolutions and max-pooling, a construction similar to deep convolution nets. Here, convolution is done at patch-level, which proceeds in a multi-layer fashion. In this multi-layered architecture, the images are subdivided into patches like a quad-tree pattern, but the quadrants in the target image are not in fixed positions. Hence, these sub-blocks are allowed to move locally to re-optimize their position, irrespective of the position of other sub-patches. In this way, each of the 16 sub-patches in a 4*4 grid can move and match to the position from which it finds a closest match.

5.1 Building of the approach

This algorithm starts to generate the correlation maps in a bottom up fashion and later computes the correspondence in a top down fashion. The SIFT/HOG descriptor which is a popular approach to match regions between images, with 4×4 spatial cells generates a real vector in 128 dimensional space $V \in \Re^{4\times4\times8}$. Now the SIFT patch can be split into 4 quadrants represented as $I = [I^0, I^1, I^2, I^3]$ with $I^n \in \Re^{2\times2\times8}$. Suppose, there are two SIFT descriptors – one reference and another target. In the target descriptor, the quadrants of 4×4 sized grids have not been kept fixed. Their positions can be optimized by maximizing $Sim(I, I'(p)) = \frac{1}{4}\sum_{i=0}^{3} \max_{p_i} sim(I_i, I'(p_i))$, where $I'(p) \in \Re^{2\times2\times8}$ is the descriptor of a single quadrant extracted at position p. The similarity can be estimated efficiently with the assumption that each of these quadrants can move independently (upto some extent), which gives a coarse non-rigid matching. This method can perform reasonable non-rigid matching with explicit pixel-wise correspondences, if it is applied in recursive nature, which

motivates to use Deep Matching in FKP matching problem. For the sake of clarity, the matching algorithm is divided into two main steps.

– Correlation maps are computed 23using a bottom-up algorithm.
– A top-down method estimates the motion of atomic patches starting from matches of large patches.

5.2 DeepKnuckle : matching algorithm

In this section, we introduce a matching algorithm based on correlations at patch-level. Two given images I_R and I_T are compared using algorithm 6. Initially, the algorithm works in a bottom-up fashion (fine level to coarse-level) which include convolution, max-pooling and sub-sampling as depicted in Fig. 11. It starts with the computation of correlation maps of small sized patches and proceeds up to larger patches by aggregating the smaller patches. Finally, a top-down method is implemented to estimate the motion of atomic patches starting from top level correlation maps. Each response map has maxima which alone cannot explain the full set of pixel-wise correspondences between the images so that the correspondences extracted from all local maxima are merged in order to better estimate the global flow. In this way, after using deep matching the number of feature points matched correctly can be used as a matching score. In this work, we have used its inverse as a dis-similarity score. Finally,

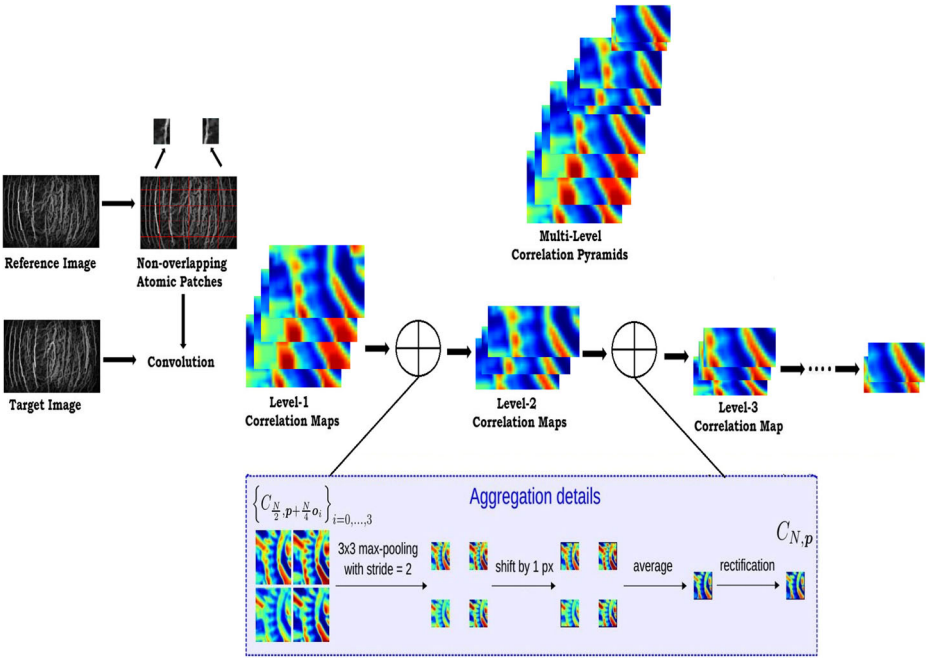

Fig. 11 Correlation maps obtained while matching reference image with target image using DeepMatching [34]

a top-down method is implemented to estimate the motion of atomic patches starting from top level correlation maps as depicted in Fig. 12. All parameters used in DeepMatching, have been listed and their default values with descriptions, as well as operating ranges are presented in Table 2.

Algorithm 6 DeepMatching

Require:
Two FKP sample images, (a) Reference image I_R, and (b) Target Image I_T of size $m \times n$.
Ensure: Return a Similarity score between given two images.
1: Divide I_R into atomic patches of size 4×4 pixels.
2: Compute correlation map $C_{4,p} = I_{R(4,p)} * I_T$ between each atomic patch in I_R and whole I_T recursively, where p= N > 4, is a power of 2.
3: Aggregate correlation maps of four $\frac{N}{2} \times \frac{N}{2}$ sized atomic patches to create a $N \times N$ size larger patch.
4: Perform max-pooling over $M \times N$ sized correlation map at each level by sliding 3×3 sized grid and filling the corresponding max-values in each $N_1 \times N_2$ sized atomic patch.
5: Perform sub-sampling to reduce the non-maximal values as well as the time complexity.
6: Shift each correlation map by one pixel and compute the shifted average of those correlation map.
7: Apply non- linear mapping function (γ rectification) to increase the range of correlation values at each level.
8: Compute multilevel correlation pyramid $(C_{N,p})_{N,p}$ which represents the average similarity score between two images.
9: Set a tolerating scaling factor (0.5 to 2.5) and rotation in the range (-26 to +26)
10: Perform backtracking for undoing aggregation so as to recover corresponding matching points of atomic-patches at lower level.
11: Find local maxima (M_1) from each correlation map at each level and then find the next local maxima (M_2) in the neighbourhood of M_1.

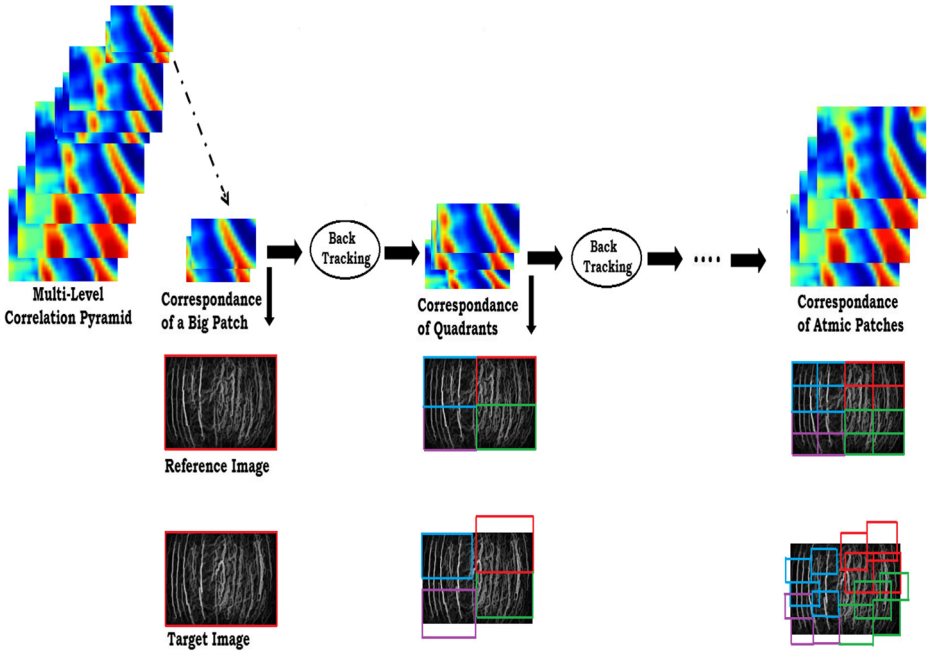

Fig. 12 Top down correspondence pruning over correlation map pyramid

6 Experimental results

Any identification or verification algorithm is tested to evaluate its performance over a data set to check its adaptability in a variety of applications. In this work, the largest benchmark publicly available, PolyU FKP dataset [1] has been used for performance evaluation. The rigours tests are performed to determine the practicality of FKP images for a biometric system.

6.1 Database specification

The database was developed by Biometric Research Center (UGC/CRC) at the Hong Kong Polytechnic University and is freely available for academic, non-commercial use. It contains 7920 images in BMP image format with resolution 110×220. The 165 $(125 : 40)$ individuals participated in the enrollment process, including males and females. For each subject, 6 images per index/middle finger are acquired in two different sessions (time gap between 14 to 96 days).

6.2 Parametric analysis

The proposed system employs multiple techniques that can module wise perform several essential tasks for effective and efficient FKP matching. Proposed techniques like BOP, SOP, IRT, Deep-Matching, ROI extraction, and local enhancement, multiple key parameters to be determined initially so as to let this system work. We have generated a small validation data set consisting of 80 subjects by considering first 20 subjects from each finger LI, LM, RI, RM. The best performing parametric set has been chosen in terms of CRR, and EER as shown in Table 2.

In Table 2, each and every parameter used in this work has been described. Its default value and operating range has been also been specified. Based on the operating range and its default value, a semantic label from the set $\{High, Moderate, Low\}$, has also been allotted. These labels can significantly enhance user's qualitative parametric understanding and reproducibility of results over different databases and scenarios.

6.3 Testing protocol

The performance metrics used for analysis of the proposed system are Equal Error Rate(EER), Correct Recognition Rate (CRR), Error under ROC Curve EUC, and Decidability Index (DI) along with computation time. The strategy is tested over inter-session matching that considers first six images as training and last six images for testing. Based on the matching score, a matching is declared genuine if both the images belong to the same class else considered as an impostor.

6.4 ROC based analysis

For a better justification of the proposed method, experiments related to recognition and verification are thoroughly conducted. The results for ROC based analysis are presented below:

Test 1: In this experiment, four categories of PolyU FKP database – Right Index (RI), Right Middle (RM), Left Index (LI), Left Middle (LM) – are considered

independently. The corresponding ROC characteristics for each category of database are shown in Fig. 13. Based on the testing protocol of our system, total of 5,940 genuine and 9,74,160 impostor matches are reported. The main conclusions from the first test are as follows. The KCP_{lBOP} based schemes gave significant improvement in results over KCP_{lSOP} transformation because FKP image patterns are better justified in BOP based longitudinal gradient. The multi-feature fusion outperforms individual feature based schemes when tested over individual FKP data sets as mentioned in Table 3. Among all four datasets, one can observe that the optimum EER of 0.96 % and CRR of 100 % are achieved with LM (165 subjects) images.

Test 2: In the second test, all subjects (660) and their corresponding poses ($660 * 12$) are included for performance evaluation. A similar methodology is adopted for

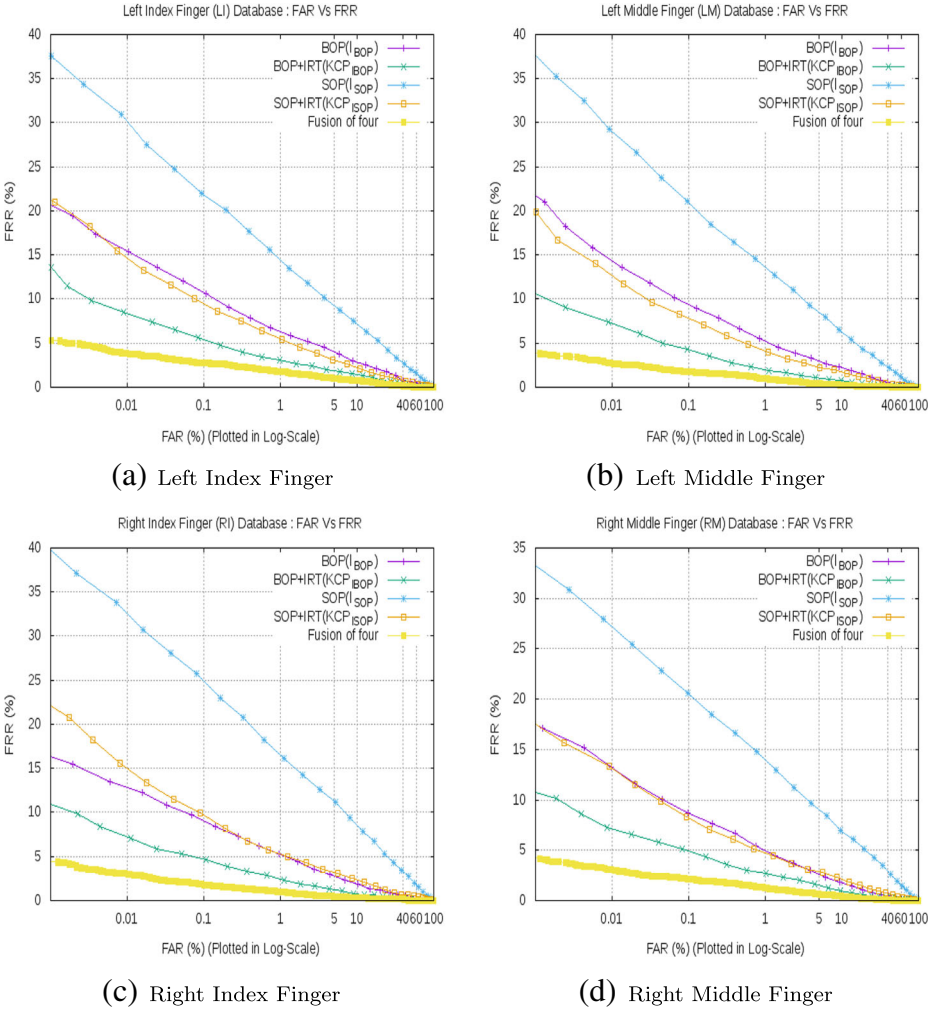

(a) Left Index Finger (b) Left Middle Finger

(c) Right Index Finger (d) Right Middle Finger

Fig. 13 Test-1 : ROC Curve based Experimental Analysis

Table 3 ROC based Performance Analysis over individual FKP databases

Description	DI	EER(%)	Accuracy(%)	EUC	CRR(%)
Left Index finger-knuckle-print PolyU Database					
l_{BOP}	2.24	4.12	96.376	1.3027	98.68
KCP_{lBOP}	2.33	2.50	97.978	0.5765	99.39
l_{SOP}	1.88	8.84	93.056	3.340	96.36
KCP_{lSOP}	2.29	3.42	96.807	1.040	98.78
$fusion$	3.40	1.10	98.722	0.261	99.39
Left Middle finger-knuckle-print PolyU Database					
l_{BOP}	2.26	3.66	96.992	0.904	99.29
KCP_{lBOP}	2.37	1.74	98.511	0.296	100
l_{SOP}	1.9120	6.97	93.449	2.868	96.86
KCP_{lSOP}	2.404	2.96	97.438	0.727	99.39
$fusion$	3.44	0.96	99.015	0.094	100
Right Index finger-knuckle-print PolyU Database					
l_{BOP}	2.35	3.17	96.972	0.836	99.09
KCP_{lBOP}	2.43	1.84	90.254	0.350	100
l_{SOP}	1.80	8.71	92.075	3.963	94.64
KCP_{lSOP}	2.29	3.57	96.865	1.050	99.59
$fusion$	3.51	0.98	99.151	0.145	100
Right Middle finger-knuckle-print PolyU Database					
l_{BOP}	2.32	3.44	97.113	0.768	99.69
KCP_{lBOP}	2.42	1.99	98.197	0.441	99.39
l_{SOP}	1.911	7.38	93.189	3.366	99.56
KCP_{lSOP}	2.319	3.64	97.124	0.942	99.29
$fusion$	3.51	0.97	98.97	0.149	99.79
Full FKP finger-knuckle-print PolyU Database					
l_{BOP}	2.32	3.13	97.088	0.8323	98.81
KCP_{lBOP}	2.36	1.93	98.42	0.339	99.62
l_{SOP}	1.911	7.35	93.18	3.366	96.45
KCP_{lSOP}	2.268	2.93	97.393	0.789	98.86
$fusion$	3.304	0.92	99.061	0.1414	99.39

selection of training and test images per class. Thus, a total number of 15,657,840 impostor and 23,760 genuine matching scores are computed. The results for complete FKP data set are described in Table 3 and ROC plots are shown in Fig. 14a. The proposed multi-feature fusion scheme achieves 0.92 % EER over full FKP data-set which is significantly higher than four individual feature based schemes. Hence, it can be concluded that our experimental results on PolyU FKP database using proposed multi-feature fusion with Deep Matching are highly robust for FKP based biometric systems. The genuine against impostor score distribution has been presented in Fig. 14b for fusion scheme over full FKP database. A well discriminating characteristic can be observed, as also reported in terms of discriminating index ($DI = 3.304$) in Table 3.

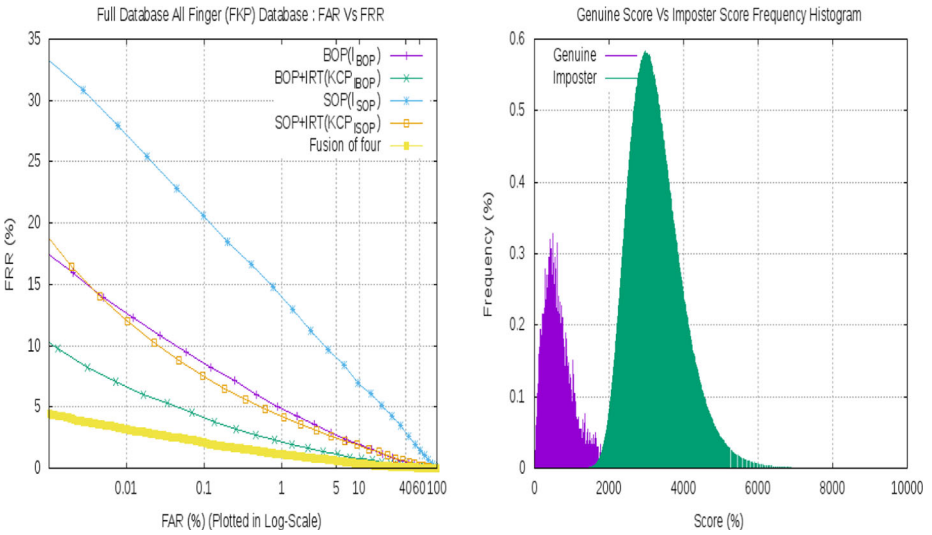

(a) ROC for full FKP database (b) Gen. Vs Imp. Score Distr. (Final Fusion)

Fig. 14 Test-2 : ROC curve based experimental analysis (Full FKP Database)

6.5 Comparative analysis with other state-of-the-art FKP systems

The performance of our proposed system is compared against some well-known systems and results has been presented in Table 4. Overall, the proposed fusion scheme has performed very well over all type of FKP images. The results presented in Table 4 strengthened our belief of suitability of FKP images for high end security purpose. The results presented for comparison are taken from [32] as public implementations are not available. One can observe that Compcode [40] and fusion of MoriCode and MtexCode [11] have been performing consistently well. But the proposed scheme has achieved superior performance. Fusion of multiple features as reported in [11] and [43] has also been surpassed by our proposed fusion, which highlights the effectiveness of our proposal. The overall performance of left hand images is slightly worse than right handed, as most of the subjects were right handed individuals.

6.6 Comparison among prevalent akin transformations

In this work, we have only considered transformations over gradient values as the performance over transformed gray values turned out to be poor as well as unfair comparison. We conclude that the vertical gradient information is more useful than the horizontal gradient for a FKP due to more prominent vertical edge structure. We have empirically observed that a 4-bit CS-LBP [13] does not achieve the high performance. Thus, we generate an 8 bit code by bit duplication. Bit redundancy have scaled the bit-code value of each pixel. It resulted in a better performance because we compute and match features over images obtained after transformation, rather than using hamming distance between codes as dis-similarity measure.

Table 4 Comparative Analysis over FKP Database (Results as reported in [32])

	Full FKP db		Left Index		Left Middle		Right Index		Right Middle	
Algorithm	EER	(%)CRR	EER	(%)CRR	EER	(%)CRR	EER	(%)CRR	EER	(%)CRR
Compcode [40]	1.386	–	1.884	–	1.883	–	1.445	–	1.175	–
BOCV [12]	1.833	–	2.202	–	2.299	–	1.892	–	1.647	–
ImCompcode+MagCode [43]	1.210	–	1.610	–	1.650	–	1.326	–	1.097	–
MoriCode [11]	1.201	–	1.544	–	1.698	–	1.605	–	1.244	–
MtexCode [11]	1.816	–	2.077	–	2.078	–	2.115	–	2.055	–
MoriCode and MtexCode [11]	1.0481	–	1.328	–	1.453	–	1.247	–	1.063	–
DeepMatching l_{SOP}	7.35	96.45	8.84	96.36	6.97	96.86	8.71	94.64	7.38	99.56
DeepMatching l_{BOP}	3.13	98.81	4.12	98.68	3.66	99.29	3.17	99.09	3.44	99.69
DeepMatching KCP_{lSOP}	2.93	98.86	3.42	98.78	2.96	99.39	3.57	99.59	3.64	99.29
DeepMatching KCP_{lBOP}	1.93	99.62	2.50	99.39	1.74	100	1.84	100	1.99	99.39
DeepMatching Proposed Fusion	0.92	99.39	1.10	99.39	0.96	100	0.98	100	0.97	99.79

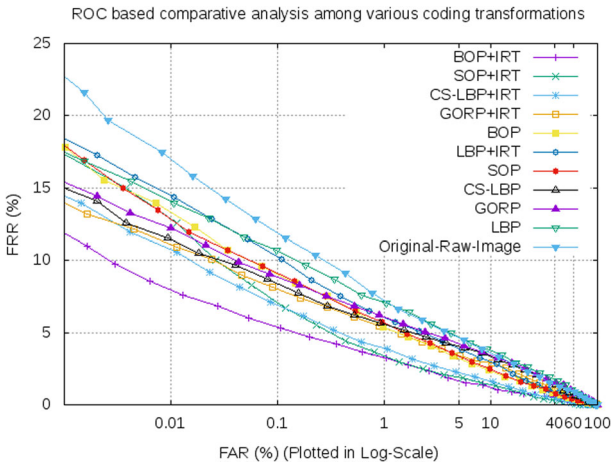

Fig. 15 Comparative analysis of various transformations such as LBP, CS-LBP *etc*. Results are obtained by applying DeepMatching over first 100 LI subjects using default parameters.

The detailed ROC based comparative analysis among prevalent akin transformations has been presented in Fig. 15. It has been observed that BOP followed by IRT has shown superior performance among all and closely followed by $SOP + IRT$. Therefore, we have fused their longitudinal components. $CS - LBP$, which is closely related to $SOP + IRT$, falls well short in performance but better then several others such as $GORP + IRT$ transformation. LBP transformation's performance has been observed to be bad as compared with others. Remaining transformations without applying IRT have also shown very similar ROC behaviour as shown in Fig. 15. Hence, such comparison helps us to conclude the superiority of the proposed DeepKnuckle based FKP framework, in which transformation BOP/SOP is followed by IRT and later matched using DeepMatching.

6.7 Time analysis

The proposed prototype system is implemented in $C/C++$ language which uses open source computer vision library $OpenCV$ along with $Torch, Atlas$ and several other libraries. The machine is equipped with four Intel(R) Core(TM) 2 Quad CPU Q9550@2.83GHz processors with a RAM of $8GB$ and open source Ubuntu 10.10 as its

Table 5 Timing Analysis

Stage	Knuckle (ms)
ROI Extraction	198
l_{BOP} and l_{SOP} Generation	$14.96 \times 2 = 29.92$
KCP_{lBOP} and KCP_{lSOP} Generation	$141.6 \times 2 = 283.2$
l_{BOP} and l_{SOP} Matching	$56.4 \times 2 = 112.8$
KCP_{lBOP} and KCP_{lSOP} Matching	$65.3 \times 2 = 130.6$
Fusion of all codes	2.3
Total Single Matching Time	756.82

operating system. The detailed time analysis of the system is reported in Table 5. The proposed system can perform single verification in less than a second (*i.e.* 756.82 ms) in our prototype system, which is fast enough for real-time applications.

7 Conclusion

This work has been carried out with the aim to develop a FKP recognition system for a rural community that can be used for applications such as financial inclusion schemes (NREGA and MNREGA). In this work, the proposed algorithm is based on score level fusion of multiple texture features. Initially, the ROI's of enhanced FKP images are extracted using modified Gabor filter method. The extracted ROI samples are further transformed using two novel BOP and SOP schemes to obtain robust image representations. The SIFT image features are matched using a hierarchical Deep matching algorithm. Deep matching performed in top down and bottom up fashion in order to handle weak texture and non-rigid deformable regions robustly. To put merit to the work, the performace is evaluated over the largest FKP benchmark dataset. The results are then compared with other state of the art methods. Our proposed methods are better in terms of CRR (99.39 %), EER (0.92 %) and computation time (756.82 ms). It has been observed that transverse features are not very useful and robust in FKP based recognition system. Also, instead of additive, a multiplicative noise assumption is better suited for such applications.

References

1. (2009) Finger-knuckle-print polyu. http://www.comp.polyu.edu.hk/biometrics
2. (2010) Biometric fingerprint quality detection. https://www.nist.gov/services-resources/software/development-nfiq-20
3. Ahonen T, Hadid A, Pietikainen M (2006) Face description with local binary patterns: Application to face recognition. IEEE Trans Pattern Anal Mach Intell 28(12):2037–2041
4. Bera A, Bhattacharjee D, Nasipuri M (2014) Hand biometrics in digital forensics, Springer, Berlin
5. Cappelli R, Ferrara M, Maltoni D (2010) Minutia cylinder-code: a new representation and matching technique for fingerprint recognition. IEEE Trans Pattern Anal Mach Intell 32(12):2128–2141
6. Cheng K, Kumar A (2012) Contactless finger knuckle identification using smartphones. In: Proceedings of the International Conference of the Biometrics Special Interest Group. IEEE, pp 1–6
7. Colbert C (1997) Knuckle profile indentity verification system. US Patent, 5,94,806
8. Cummings AH, Nixon MS, Carter JN (2011) The image ray transform for structural feature detection. Pattern Recogn Lett 32(15):2053–2060
9. Déniz O, Bueno G, Salido J, De la Torre F (2011) Face recognition using histograms of oriented gradients. Pattern Recogn Lett 32(12):1598–1603
10. Ferrer MA, Travieso CM, Alonso JB (2006) Using hand knuckle texture for biometric identifications. IEEE Aerosp Electron Syst Mag 21(6):23–27
11. Gao G, Yang J, Qian J, Zhang L (2014) Integration of multiple orientation and texture information for finger-knuckle-print verification. Neurocomputing 135:180–191
12. Guo Z, Zhang D, Zhang L, Zuo W (2009) Palmprint verification using binary orientation co-occurrence vector. Pattern Recogn Lett 30(13):1219–1227
13. Heikkilä M, Pietikäinen M, Schmid C (2009) Description of interest regions with local binary patterns. Pattern recognition 42(3):425–436
14. Jain AK, Kumar A (2010) Biometrics of next generation: an overview. Second Generation Biometrics 12(1):2–3
15. Jain AK, Ross A, Prabhakar S (2004) An introduction to biometric recognition. IEEE Trans Circuits Syst Video Technol 14(1):4–20. doi:10.1109/TCSVT.2003.818349
16. Jaswal G, Nath R, Kaul A (2015) Fkp based personal authentication using sift features extracted from pip joint. In: 3rd International Conference on Image Information Processing. IEEE, pp 214–219

17. Jaswal G, Kaul A, Nath R (2016) Knuckle print biometrics and fusion schemes–overview, challenges, and solutions. ACM Comput Surv (CSUR) 49(2):34
18. Joshi D, Rao Y, Kar S, Kumar V, Kumar R (1998) Computer-vision-based approach to personal identification using finger crease pattern. Pattern Recogn 31(1):15–22
19. Kong T, Yang G, Yang L (2014a) A new finger-knuckle-print roi extraction method based on probabilistic region growing algorithm. Int J Mach Learn Cybern 5(4):569–578
20. Kong T, Yang G, Yang L (2014b) A new finger-knuckle-print roi extraction method based on probabilistic region growing algorithm. Int J Mach Learn Cybern 5(4):569–578
21. Kumar A (2014) Importance of being unique from finger dorsal patterns: Exploring minor finger knuckle patterns in verifying human identities. IEEE Trans Inf Forensics Secur 9(8):1288–1298
22. Kumar A, Prathyusha KV (2009) Personal authentication using hand vein triangulation and knuckle shape. IEEE Trans Image Process 18(9):2127–2136
23. Kumar A, Ravikanth C (2009) Personal authentication using finger knuckle surface. IEEE Trans Inf Forensics Secur 4(1):98–110
24. Kumar A, Zhou Y (2009) Human identification using knucklecodes, IEEE
25. Kumar A, Wu C (2012) Automated human identification using ear imaging. Pattern Recogn 45(3):956–968
26. Kumar A, Wang B (2015) Recovering and matching minutiae patterns from finger knuckle images. Pattern Recogn Lett 68:361–367
27. Lowe DG (2004) Distinctive image features from scale-invariant keypoints. Int J Comput Vision 60(2):91–110
28. Monro DM, Zhang Z (2005) An effective human iris code with low complexity. In: IEEE International Conference on Image Processing, vol 3. IEEE, pp III–277
29. Morales A, Ferrer M, Travieso C, Alonso JB (2007) A knuckles texture verification method in a transformed domain. In: Proceedings of 1st Spanish Workshop on Biometrics (on CD). Girona, Spain
30. Morales A, Travieso C, Ferrer M, Alonso J (2011) Improved finger-knuckle-print authentication based on orientation enhancement. Electron Lett 47(6):380–381. doi:10.1049/el.2011.0156
31. Nigam A, Gupta P (2013) Quality assessment of knuckleprint biometric images. In: IEEE International Conference on Image Processing. IEEE, pp 4205–4209
32. Nigam A, Tiwari K, Gupta P (2016) Multiple texture information fusion for finger-knuckle-print authentication system. Neurocomputing 188:190–205
33. Ravikanth C, Kumar A (2007) Biometric authentication using finger-back surface. In: IEEE Conference on Computer Vision and Pattern Recognition. IEEE, pp 1–6
34. Revaud J, Weinzaepfel P, Harchaoui Z, Schmid C (2015) Deepmatching: Hierarchical deformable dense matching. Int J Comput Vis:1–24
35. Sanchez-Reillo R, Sanchez-Avila C, Gonzalez-Marcos A (2000) Biometric identification through hand geometry measurements. IEEE Trans Pattern Anal Mach Intell 22(10):1168–1171
36. Woodard DL, Flynn PJ (2005) Personal identification utilizing finger surface features. In: IEEE Computer Society Conference on Computer Vision and Pattern Recognition, vol 2. IEEE, pp 1030–1036
37. Yu PF, Zhou H, Li HY (2014) Personal identification using finger-knuckle-print based on local binary pattern. In: Applied mechanics and materials, vol 441. Trans Tech Publ, pp 703–706
38. Yu H, Yang G, Wang Z, Zhang L (2015) A new finger-knuckle-print roi extraction method based on two-stage center point detection. International Joumal of Signal Processing, Image Processing and Pattern Recognition 8:185–200
39. Zaw KP, Kbaing AS (2014) Implementation of contactless finger knuckle identification system. International Joumal of Science. Engineering and Technology Research 3(6):1599–1605
40. Zhang L, Zhang L, Zhang D (2009) Finger-knuckle-print: a new biometric identifier. In: 16th IEEE International Conference on Image Processing. IEEE, pp 1981–1984
41. Zhang L, Zhang L, Zhang D (2010a) Monogeniccode: A novel fast feature coding algorithm with applications to finger-knuckle-print recognition. In: International Workshop on Emerging Techniques and Challenges for Hand-Based Biometrics. IEEE, pp 1–4
42. Zhang L, Zhang L, Zhang D, Zhu H (2010b) Online finger-knuckle-print verification for personal authentication. Pattern Recogn 43(7):2560–2571
43. Zhang L, Zhang L, Zhang D, Zhu H (2011) Ensemble of local and global information for finger-knuckle-print recognition. Pattern Recogn 44(9):1990–1998

Gaurav Jaswal received B.Tech degree in Electronics and Communication Engineering from Green Hills Engineering College, Solan, India in 2007, M.Tech degree in Electrical Engineering from National Institute of Technology, Hamirpur, India in 2010. He is currently pursuing Ph.D degree from National Institute of Technology, Hamirpur, India. His research interest includes Pattern Recognition, Image Processing, and Multimodal Biometrics.

Aditya Nigam received Ph.D. and M.Tech. degrees in Computer Science and Engineering from Indian Institute of Technology Kanpur (IITK), India, in 2015 and 2009 respectively. He is currently working as an Assistant Professor in the School of Computing and Electrical Engineering at Indian Institute of Technology Mandi, India. His research interest includes Biometrics, Pattern Recognition, Computer Vision and Image Processing.

Ravinder Nath received BE degree in Electrical Engineering from Madan Mohan Malviya Engineering College, Gorakhpur, India in 1987, M.Tech degree in electrical engineering from National Institute of Technology, Kurukshetra, India in 1991 and Ph.D degree in Electrical engineering from Indian Institute of Technology, Kanpur, India in 2006. He joined REC Kurukshetra as a lecturer in year 1989 and then NIT Hamirpur (formerly known as REC Hamirpur) in year 1990. Currently he is working as Associate Professor in the department of electrical engineering, National Institute of Technology, Hamirpur, India. His research interests include signal processing, communication systems, and control systems.